ACS Energy LETTERS

Cite This: ACS Energy Lett. 2018, 3, 1279−1286

LETTER

Interplay of Mobile Ions and Injected Carriers Creates Recombination Centers in Metal Halide Perovskites under Bias

Susanne T. Birkhold,[†,§] Jake T. Precht,[†] Hongbin Liu,[†] Rajiv Giridharagopal,[†] Giles E. Eperon,[†,#] Lukas Schmidt-Mende,[‡] Xiaosong Li,[†] and David S. Ginger*[,†]

[†]Department of Chemistry, University of Washington, Seattle, Washington 98195, United States

[‡]Department of Physics, University of Konstanz, 78464 Konstanz, Germany

[#]Cavendish Laboratory, JJ Thomson Avenue, Cambridge CB3 0HE, United Kingdom

Supporting Information

ABSTRACT: We study the interaction of mobile ions and electronic charges to form nonradiative defects during electric biasing of methylammonium lead triiodide ($MAPbI_3$) and formamidinium lead triiodide ($FAPbI_3$) thin films. Using multimodal microscopy that combines in situ photoluminescence and scanning Kelvin probe microscopy in a lateral electrode geometry, we correlate temporal changes in radiative recombination with the spatial movement of ionic and electronic charge carriers. Importantly, we compare trap formation with both charge injecting and blocking contacts. Even though ion migration takes place in both cases, we observe the formation of new nonradiative defects in $MAPbI_3$ only in the presence of injected electrons, suggesting that redox processes play a key role. On the basis of density functional theory (DFT) simulations, we propose that reduction of Pb^{2+} to Pb^0 is responsible for the new defects formed in our films. These results underscore that defect properties in metal halide perovskites are not only determined by the migration of mobile ions but are also highly sensitive to their interaction with injected electronic charge.

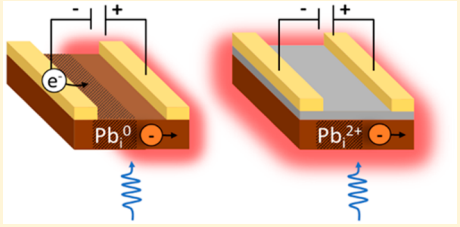

Despite the rapid progress in the performance of perovskite solar cells, questions about their commercial viability remain. In particular, reports of changing composition and performance during device operation due to dynamic processes demand an improved understanding of the influence of illumination and electrical bias on metal halide perovskites.[1,2] Several experimentally observed phenomena in methylammonium lead iodide ($CH_3NH_3PbI_3$, abbreviated as $MAPbI_3$) have been attributed to the formation of defects and their ability to migrate within the crystal lattice. These effects range from current−voltage hysteresis to a switchable photovoltaic effect and light-induced changes of optical and electronic properties.[3−6] While it is now accepted that the mixed ionic−electronic conductivity[7] combined with low defect formation energies[8] can give rise to the complex transient responses of metal halide perovskites with time scales of 10^{-3}−10^3 seconds,[9−12] the interplay of these factors is still poorly understood.

Slow changes in emission properties, including photoinduced halide segregation,[13,14] increases in photoluminescence (PL) intensity,[15,16] and bias-induced PL quenching, have been associated with the motion of ions and demonstrate the sensitivity of emission properties to local stoichiometry. Poling experiments on $MAPbI_3$ with lateral electrodes revealed both reversible and irreversible motion of ions under applied electric fields, and the decrease in PL intensity observed close to the electrodes[17−19] has been interpreted as trap formation primarily due to ion motion. The nature of these field-induced nonradiative recombination centers is still unclear as most defect energies for mobile ionic species, like interstitials or vacancies of iodide and methylammonium, are assumed to be shallow.[20−22] Recent reports have further emphasized that the charge carrier population impacts the intimate relationship between ion migration and nonradiative recombination pathways.[6,23] The collective action of ionic and electronic charges during electric poling is also assumed to be a major cause of current−voltage hysteresis and calls for an improved understanding of the impact of simultaneous ion migration and charge trapping on recombination mechanisms.[23−26]

Here, we investigate the role of ion migration and charge injection on trap formation during electrical poling. To better disentangle the roles of ionic and electronic motion, we study the PL quenching of $MAPbI_3$ using lateral devices with both charge injecting and blocking (insulator-coated) contacts. In

Received: March 28, 2018
Accepted: May 7, 2018
Published: May 7, 2018

DOI: 10.1021/acsenergylett.8b00505
ACS Energy Lett. 2018, 3, 1279−1286

situ observations of ion migration by time-resolved PL and scanning Kelvin probe microscopy (SKPM) allow a direct correlation between the formation of nonradiative recombination centers and the distribution of charge carriers. We show that bias-induced ion motion itself in $MAPbI_3$ does not necessarily result in the creation of nonradiative recombination centers, as has previously been claimed, but that the combination of charge injection and ion motion is more effective at creating defects that serve as nonradiative recombination centers. Combining these experimental results with ab initio calculations, we propose that these dynamic defects are reduced Pb^0 sites in $MAPbI_3$. Our calculations predict that these defects are more benign in formamidinium lead iodide films, $(HC(NH_2)_2PbI_3$, abbreviated as $FAPbI_3$), and our experiments confirm that combining bias and electrical injection in $FAPbI_3$ results in much lower levels of PL quenching, providing a self-consistent picture of the bias- and injection-induced defect formation in both $MAPbI_3$ and $FAPbI_3$ under pure poling, or combined poling and injection conditions, across multiple perovskite families.

We studied ion motion and trap formation using lateral junctions that allow us to profile local surface potentials via SKPM while simultaneously probing local changes in nonradiative recombination rates due to trap formation via PL. To test if changes in nonradiative decay rates are induced solely by ion motion or depend on charge injection, we compared surface potential and PL profiles for injecting and insulator-coated contacts. The experimental geometry is depicted in Figure 1a. Although PL and SKPM measurements probe the sample from the top and bottom, respectively, a comparison of the two image modalities is fair in our samples as reported carrier diffusion lengths of 100−2000 nm are comparable to our film thickness (~250 nm)[27−30] and SKPM measurements probe the charge distribution over a thickness comparable to the charge screening length of ~100 nm. Variations in the electric field strength along the film thickness are assumed to be negligible as the gap width (~10 μm) is significantly larger than the film thickness.

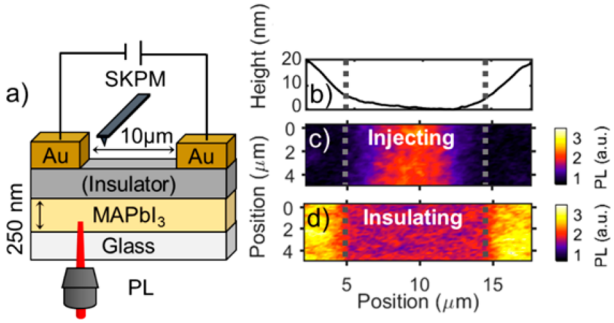

Figure 1. (a) Device geometry for PL (through glass) and scanning Kelvin probe microscopy (SKPM) measurements (at top surface). (b) Topography cross section and PL maps for (c) $MAPbI_3$/Au and (d) $MAPbI_3$/PMMA/SiO_2/Au across the electrode gap. Vertically dotted lines indicate the position of the electrode edges.

Figure 1b−d shows the topography of the 10 μm wide electrode gap and PL maps of $MAPbI_3$/Au and $MAPbI_3$/PMMA/SiO_2/Au devices prior to electric poling. These $MAPbI_3$ films are deposited by the antisolvent method without further surface treatment, producing films with PL properties comparable to common reports in the literature, though their PL lifetimes (~100 ns) are shorter than those of the very best surface-passivated materials (see Figure S1 in the SI).[31,32] In the case of injecting contacts, the PL intensity is reduced in the vicinity to the contacts due to Fermi level equilibration with the metal even prior to biasing (Figure 1c).[33] In contrast, charge injection is blocked for the insulator-coated contacts, resulting in an increased PL intensity below the electrodes due to reflection of the laser at the electrode and double-pass excitation of the perovskite (Figure 1d). All PL measurements were performed after light soaking yielded stabilized radiative recombination rates.[34] Initial increases in PL intensity during light soaking are displayed in Figure S2.

The PL maps in Figure 1c,d show a fairly homogeneous distribution of intensity throughout the electrode gap, despite small local variations, consistent with the typical PL heterogeneity of perovskites films.[35−37] Due to the relatively small grain sizes of the perovskite film of around 200 nm (topography displayed in Figure S3), the optical resolution (~500 nm) is not sensitive to specific grains but instead presents the overall distribution of PL intensity between the two electrodes. Hence, repeatedly scanning a single line across the electrode gap, as presented in Figure 2, allows a real-time observation of changes in PL intensity between the electrodes. The vertical "features" in these images result from consecutive lateral scanning over the same slightly heterogeneous lateral line profile (the y-axis is time, not position).

PL Measurements during and after Electric Poling. In Figure 2a,c, application of +9 V bias to the right electrode, while the left electrode is grounded, yields an electric field of 0.9 V/μm, which is similar to fields encountered in working perovskite solar cells. Figure 2a shows the change in PL intensity of a $MAPbI_3$/Au device during such electric poling. Similar to previous observations,[19,24] the total PL intensity is instantly reduced by around 20% when the bias is applied as the electric field and direct contacts promote separation and extraction of photogenerated charges.[38] More interestingly, nonuniform PL quenching occurs at the negative electrode and starts to propagate toward the positive electrode on a time scale of ~1200 s. After electric poling, both electrodes are grounded and the PL intensity slowly and reversibly recovers over approximately 900 s (Figure 2b). As PL quenching and recovery feature a continuously propagating front, we propose that a migration of charged ions from one electrode to another causes changes in the PL intensity. These results are similar to the report by Zhang et al., who observed reversible PL quenching in $MAPbI_3$ from the negative toward the positive electrode on similar time scales.[33] Likewise, electric poling measurements by Jacobs et al. were reported to produce PL quenching around the negative electrode, yet in their case PL quenching was irreversible.[24] Importantly, these[24,33] and other studies[17,19] have primarily interpreted bias-induced PL quenching in perovskites in the context of field-induced ion migration. Next, we show here that charge injection is a critical component of this quenching process.

Figure 2c,d shows what happens when the same biasing experiment is performed using insulator-coated contacts that can pole the sample with an applied field but not inject or extract carriers. Notably, Figure 2c,d shows that no quenching occurs in $MAPbI_3$ films in this case. This experiment indicates that the reversible trap formation observed when biasing $MAPbI_3$ films (Figure 2a,b) requires charge injection, *not just field-induced ion motion*. As the gap width (~10 μm) is significantly larger than the insulator thickness (~80 nm), only

DOI: 10.1021/acsenergylett.8b00505
ACS Energy Lett. 2018, 3, 1279−1286

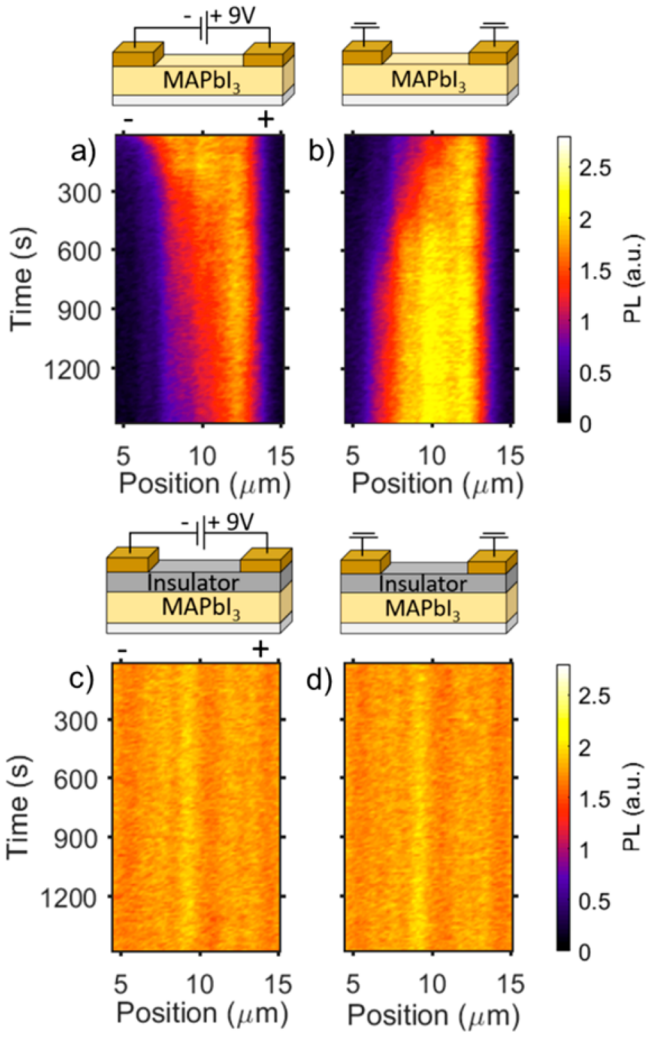

Figure 2. PL scan of a single line within the electrode gap for (a,b) $MAPbI_3$/Au and (c,d) $MAPbI_3$/PMMA/SiO_2/Au during (a,c) a bias of +9 V applied to the right electrode and (b,d) after bias. Above each measurement, schematic illustrations display the used device configuration.

minor potential drops are expected to occur at the insulating layer (~0.1 V), as confirmed by SKPM profiles. We therefore exclude that the absence of PL quenching in insulator-coated devices is due to a smaller electric field. This claim is further verified by the fact that the entire 9 V is observed to drop across the 10 μm wide junction (Figure 3d) and tested biases up to 20 V on insulator-coated devices do not cause any changes in the PL either (Figure S4). Additionally, as all bias-induced changes were found to be reversible even without application of a reversed electric field, we do not believe that field-induced migration of metallic gold into the perovskite layer causes the differences between direct and insulator-coated electrodes.

Control measurements that exclude the impact of the insulating layer's encapsulating properties on the PL quenching mechanism are included in the SI (Figure S5). To examine possible differences in the mechanism of ion migration for injecting and blocking contacts, we next consider changes in the surface potential using SKPM.

Kelvin Probe Measurements during and after Electric Poling. SKPM has proven to be extremely useful for the investigation of electric-field-driven ion migration between lateral electrode structures.[4,5,33,39−43] In general, Kelvin probe measures the contact potential difference (CPD) between the work functions of the tip and sample ($V_{CPD} = (\phi_{tip} - \phi_{sample})/-e$) and is affected by changes in the charge distribution in the film, e.g., due to doping or localized charged surface defects, as illustrated in Figure S6. The potential displayed in Figure 3 is the DC bias V_{DC} that is applied to the tip to nullify the CPD with $V_{DC} = -V_{CPD}$.[39,40,44]

Figure 3a−c shows the evolution of the SKPM signal over time within the electrode gap for charge injecting contacts during and after electric poling of $MAPbI_3$/Au devices. During electric poling, the applied potential of 9 V drops uniformly across the electrode gap. With time, a minor shift of this potential drop toward the positive electrode takes place. After removing the bias, the SKPM signal is increased by around +200 mV close to the negative electrode relative to the initial profile, which is consistent with an upward Fermi level shift in this region, as one would expect from an increased concentration of electrons near the negatively biased contact (Figure 3b,c). This increased SKPM signal dissipates slowly but does not fully recover to its initial state within the ~1500 s time frame that we measure here (Figure 3b,c). Similar increases of the SKPM signal close to the electrodes after electric poling have already been reported for $MAPbI_3$/Au devices and have been interpreted as doping of the perovskite film.[4,5,33] This doping has previously been assigned to an accumulation of charged defects close to the electrodes that causes electronic charge injection into the perovskite film to maintain charge neutrality. We interpret this data as an indication that during electric poling mobile ions migrate across the electrode gap. This ion motion, together with charge carrier injection from the electrodes, leads to a net increase in negative carrier density in the film after biasing. There appears to be only a slight difference in the behavior of positive and negative species at the negative/positive electrodes, in this case.

Insulator-coated contacts prevent the injection of large concentrations of electronic carriers and hence allow a more direct observation of intrinsic ionic and electronic charge motion (Figure 3d−g). With insulator-coated contacts, we observe that during bias the potential is initially partly screened within the electrode gap with a symmetric potential drop at both electrodes (Figure 3d). This electrolytic-capacitor-like potential drop then evolves into a more insulator/resistor-like behavior with a constant electric field distribution in the junction within the first 400 s, and we can see the entire 9 V potential drop across the electrode gap. On the basis of the fast time scales involved, we propose that the unintentional electronic doping of the perovskite film at the level of ~10^{14}−10^{15} cm^{-3} (see SI, Figure S7 and corresponding discussion) leads to the observed initial charge accumulation and potential screening at the insulator-coated contacts as charges cannot be injected or extracted.[45] On slower time scales, ions start to migrate toward the electrodes, causing a redistribution of the field and carriers within the film to restore neutrality. Notably, when scanning the potential after the bias is removed, we observe significant residual negative and positive potential peaks of over 2 V close to the positive and negative electrode, respectively (Figure 3e,f). This potential shift is much larger than in the presence of injected carriers. We assign these potential peaks to the accumulation of charged mobile ions. Figure 3g displays the net charge carrier density, $\delta(x)$, extracted from the potential profile $\varphi(x)$ through application of the Poisson equation

DOI: 10.1021/acsenergylett.8b00505
ACS Energy Lett. 2018, 3, 1279−1286

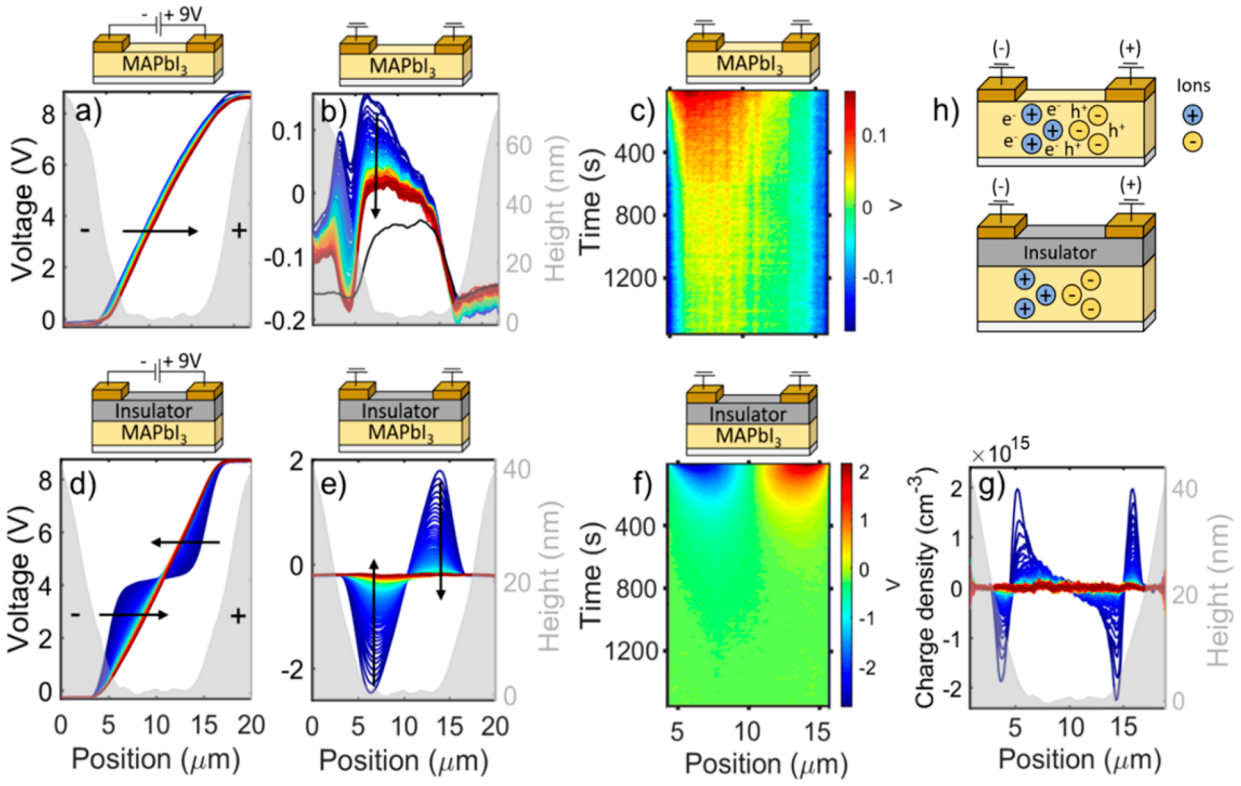

Figure 3. SKPM scan of a single line within the electrode gap of (a−c) $MAPbI_3$/Au and (d−f) $MAPbI_3$/PMMA/SiO_2/Au, measured (a,d) with a +9 V bias applied to the right electrode and (b,c,e,f) at 0 V bias after turning off the +9 V bias. The black line in (b) displays the SKPM CPD signal prior to biasing. (g) Charge density in $MAPbI_3$/PMMA/SiO_2/Au after bias. (h) Illustration of electronic and ionic charge distribution after electric biasing. The CPD sign convention is such that more positive bias applied to the tip corresponds to a shallower (more n-type) work function. Each line presents a line scan with 12 s time resolution, and arrows depict the temporal evolution. Shaded areas show the topography of the electrode gap.

$$\frac{\partial^2 \varphi}{\partial x^2} = \frac{1}{\varepsilon_r \varepsilon_0}\delta(x)$$

as it is commonly done in lateral SKPM experiments.[39,43,46] Here, ε_0 is the vacuum permittivity and ε_r the relative dielectric constant (we take the static ε_r = 25 for the perovskite).[47] The resulting charge density of ∼2 × 10^{15} cm^{-3} is compatible with reported defect densities in $MAPbI_3$ films.[15,48] We note that this charge density presents a net charge density of electronic and ionic carriers as a partial screening of ionic charge by intrinsic, oppositely charged electronic carriers is expected. Therefore, the measured net charge density in Figure 3g is assumed to provide a lower limit of redistributed ionic density after poling.

As displayed in Figure 3g, the extracted net charge density is highest at the electrode edges and decays toward the gap center with an exponential decay length of approximately 700 nm. Here, we note that factors like defects in the insulating layer,[49] deviations between bulk and surface charge densities, as well as the choice of dielectric constant might affect the accuracy of the extracted charge density, but in all cases, these factors would lead to underestimation of the potential and ion densities relative to those measured with injecting contacts. In other words, our qualitative conclusions will remain unaffected and are in fact strengthened by these considerations.

Figure 3e,f shows the relaxation of the potential profile after removal of the bias and shorting of the contacts. The potential takes several hundred seconds to return to its initial condition, a time scale consistent with ionic motion, deep trapping of carriers, or both. The similar density and decay kinetics of oppositely charged ionic defects at each electrode suggests a paired origin of positive and negative mobile ions, e.g., some particular species of vacancies and their equivalent interstitials. Figure 3h summarizes the proposed electronic and ionic charge distribution after biasing for charge injecting and insulating device configurations.

Comparing Figure 3a−c and Figure 3d−f for charge injecting and blocking contacts, respectively, shows that the dynamics of ion migration are slowed if charges are injected. We propose that ions that are accompanied by charge carriers of opposite sign have slower dynamics due to a reduced drift under an electric field. We therefore conclude that ion migration is taking place both with and without charge injecting contacts; however, as migrating ions have different amounts of screening, their dynamics and impact on the CPD vary.

Origin of PL Quenching. Importantly, the results presented in Figure 2 show that in our $MAPbI_3$ films an increase in the density of nonradiative recombination centers occurs under bias only for injecting contacts, not for insulator-coated contacts. Perhaps surprisingly, this data indicates that bias-induced ion motion alone, at least at the biases/concentrations probed herein, does not necessarily produce a large increase in the density of deep traps. We next turn to discuss the origins of PL quenching in the $MAPbI_3$ films with injecting contacts.

Figure 2a shows that the PL quenching proceeds beginning at the negative (electron injecting/hole extracting) contact in our lateral devices. This result suggests that the accumulation of positive ions and/or depletion of negative ions and,

DOI: 10.1021/acsenergylett.8b00505
ACS Energy Lett. 2018, 3, 1279−1286

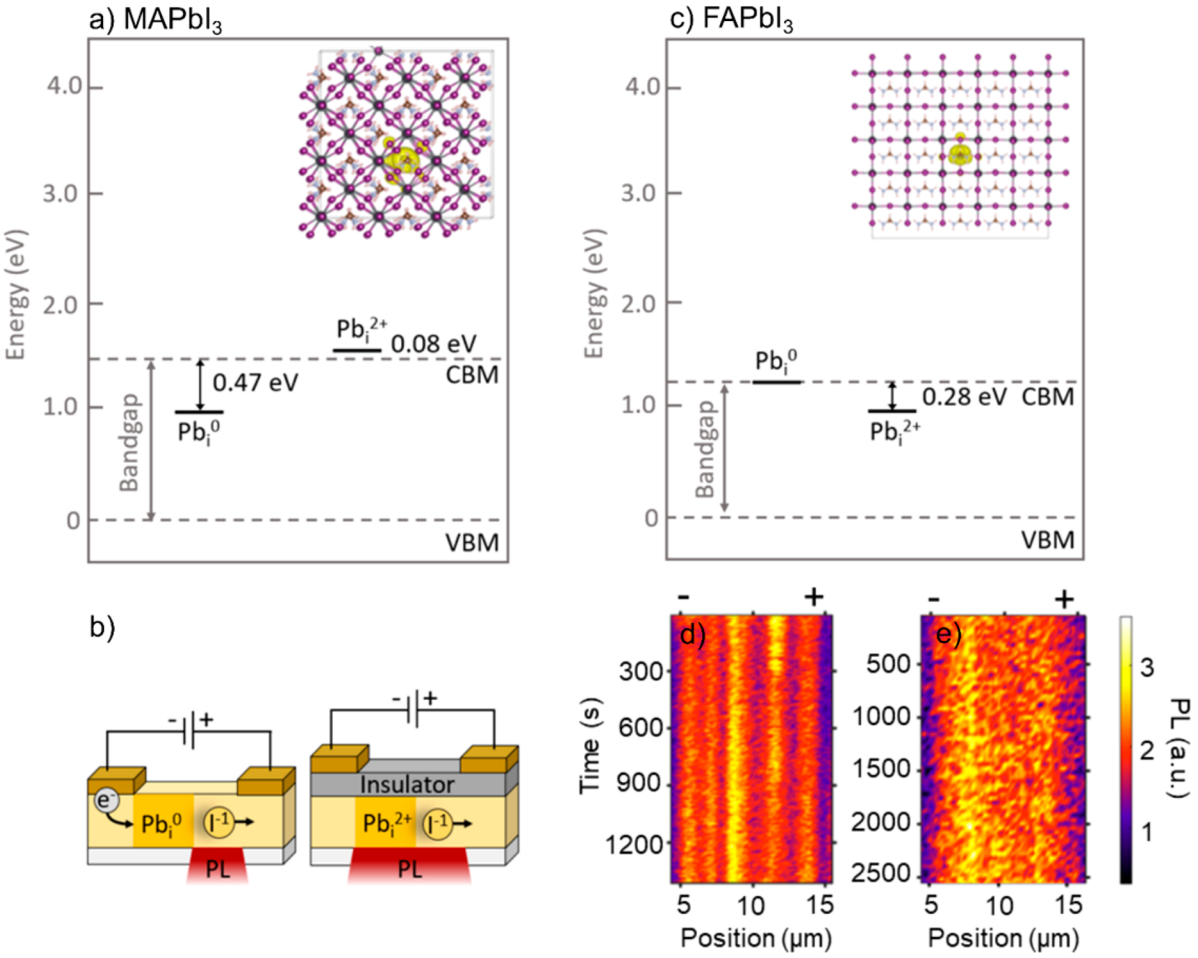

Figure 4. (a) Calculated energy levels of lead interstitials in $MAPbI_3$. (b) Schematic illustration of the PL quenching mechanism in $MAPbI_3$. (c) Calculated energy levels of lead interstitials in $FAPbI_3$. Insets show calculated orbitals of the supercells with defect Pb_i^0. PL line scans of (d) $FAPbI_3$/Au and (e) $FAPbI_3$/PMMA/SiO_2/Au during a bias of +9 V applied to the right electrode.

importantly, the electrochemical reduction of some species due to charge injection near the negative electrode are the likely origin of the PL quenching. With respect to possible sources, we consider iodide vacancies, methylammonium interstitials, and lead interstitials as possible candidates based on literature reports.[20,32,50] Simulations, however, suggest that the energies of methylammonium interstitials and iodide vacancies are insensitive to their charge state, whereas the trap depths of Pb interstitials are reported to be sensitive to their charge.[20,51] Given the role of charge injection, we thus consider the possibility that the varying redox state of lead defects is responsible for the differences in trap behavior observed between our samples with charge injecting and charge blocking contacts.

We therefore carried out ab initio calculations to determine the expected trapping levels of lead-based defects. Details of the calculation procedure are given in the SI and Figures S8–S10. Figure 4a displays the calculated defect energy levels of lead interstitials Pb_i centered within a 3 × 3 × 3 $MAPbI_3$ supercell. As recent reports have shown that energy levels of lead interstitials are sensitive to their charged state,[20,34,50] we calculated the energies of both Pb_i^{2+} and Pb_i^0. The resulting energy levels predict that ionic Pb_i^{2+}, with a defect energy level 0.08 eV above the conduction band minimum (CBM), forms no trap state. However, our calculations predict that reduction of Pb_i^{2+} to Pb_i^0 creates a deep trap state with a defect energy level 0.47 eV below the CBM, in agreement with the calculations by Buin et al.[20]

We consider Pb_i^0 as a plausible nonradiative defect in our biased films: the existence of metallic lead Pb^0 in $MAPbI_3$ films has already been confirmed by XPS measurements,[52−56] and its occurrence has been correlated with an understoichiometry of iodide,[52] as could develop under electrical poling. Furthermore, Pb^0 defects have been shown to be a source of nonradiative trap states that reduce PL quantum efficiency, as well as solar cell device performance.[55,56] We therefore speculate that iodide, which has been confirmed to be the most mobile species in $MAPbI_3$,[57] migrates toward the positive electrode during electric poling, causing the formation of lead-related defects close to the negative electrode (illustrated in Figure 4b). Our defect calculations predict that such lead defects form deep trap states if concomitant electron injection enables reduction of Pb_i^{2+} into Pb_i^0. In contrast, insulator-coated contacts prevent the interaction of injected charges and lead interstitials, resulting in Pb_i^{2+} defects that are expected to be more electronically benign. Thus, attributing the PL quenching we observe to Pb_i^0 explains multiple observations in our experiments and is consistent with recent literature precedent.

$FAPbI_3$ is reported to exhibit different defect levels from $MAPbI_3$.[58] Thus, as a comparison, we calculated the defect energy levels of lead interstitials in $FAPbI_3$ using the same approach. Figure 4c shows that the calculated trap energy levels

DOI: 10.1021/acsenergylett.8b00505
ACS Energy Lett. 2018, 3, 1279−1286

change for $FAPbI_3$, with reduced energy levels of 0.003 eV for Pb_i^0 and 0.28 eV for Pb_i^{2+}. While it is difficult to calculate quantitative trap depths at this level of theory, we expect the qualitative ordering of trap energies to be consistent. In this regard, we note that the calculation predicts Pb_i^0 interstitials in $MAPbI_3$ to form defects that are both deeper than Pb_i^{2+} interstitials in $MAPbI_3$ and deeper than Pb_i^0 and Pb_i^{2+} interstitials in $FAPbI_3$. This trend is in qualitative agreement with the experimental data if we interpret our nonradiative decay to Pb_i^0 interstitial formation (see below).

Finally, we performed the same electrical poling experiments on $FAPbI_3$ films that we performed on $MAPbI_3$ films. Figure 4d,e shows PL traces under bias for both charge injecting (Figure 4d) and blocking (Figure 4e) contacts on $FAPbI_3$ films. For $FAPbI_3$, in contrast to $MAPbI_3$, we observe no PL quenching for either blocking or injecting contacts. We interpret this result as being consistent with Pb_i^0 interstitial formation as the source of nonradiative recombination in $MAPbI_3$ and with the theoretical prediction that Pb_i^0 is a deeper defect in $MAPbI_3$ than that in $FAPbI_3$, even if the exact energy of the defects does not agree between experiment and theory.

In summary, we compared PL quenching of metal halide perovskite films during electric poling with and without injecting contacts for both $MAPbI_3$ and $FAPbI_3$ thin films in a lateral electrode geometry. Independent of device configuration, a slow, field-induced ion migration is measured by SKPM. However, in these films, we only observe bias-induced PL quenching in $MAPbI_3$ films with injecting contacts but not in $MAPbI_3$ films that exhibit ion motion without charge injection nor in $FAPbI_3$ films with either blocking or injecting contacts. On the basis of calculations, we hypothesize that, following electric poling and ion migration, Pb-related defects form near the negative electrode that can either be deep or shallow trap states depending on their redox state.

Beyond this specific interpretation, these results are more broadly important because they underscore that individual probes (PL, surface potential) do not tell the entire story regarding defect formation and migration in perovskites, and therefore, multimodal approaches are increasingly necessary to understand these complex systems. Notably, it is possible that earlier studies on transients and defect formation, especially those that have been interpreted solely in terms of ion motion, should likely be re-examined in the context of the effects of injected carriers. Finally, these results hold promise for engineering the long-term stability of perovskite films: the observation that $FAPbI_3$ films are robust against bias and injection-induced PL quenching suggests that compositional and surface engineering may be able to overcome some of the instabilities of the prototypical $MAPbI_3$ perovskite semiconductor using newer formulations and by considering carrier densities and redox processes in devices.

■ ASSOCIATED CONTENT

Supporting Information

The Supporting Information is available free of charge on the ACS Publications website at DOI: 10.1021/acsenergylett.8b00505.

Description of experimental methods, detailed calculation procedure, film topography, illustration of contact potential difference, photoluminescence lifetimes, initial photoluminescence measurements upon light soaking, photoluminescence measurements with higher biases, photoluminescence measurements on the encapsulation effect of insulating layers, approximation of intrinsic electronic carrier density, and ab initio calculation results (PDF)

■ AUTHOR INFORMATION

Corresponding Author

*E-mail: ginger@chem.washington.edu.

ORCID

Susanne T. Birkhold: 0000-0003-1364-9944
Hongbin Liu: 0000-0001-9011-1182
Giles E. Eperon: 0000-0001-9600-4847
Lukas Schmidt-Mende: 0000-0001-6867-443X
Xiaosong Li: 0000-0001-7341-6240
David S. Ginger: 0000-0002-9759-5447

Present Address

§S.T.B.: Department of Physics, University of Konstanz, 78464 Konstanz, Germany.

Notes

The authors declare no competing financial interest.

■ ACKNOWLEDGMENTS

This Letter is based primarily on work supported by the DOE (DE-SC0013957). S.T.B. acknowledges financial support from the Fulbright Commission and the Carl Zeiss Foundation. J.T.P. is supported by a National Science Foundation Graduate Research Fellowship under Grant No. DGE-1256082. G.E.E. is supported by the European Union's Framework Programme for Research and Innovation Horizon 2020 (2014-2020) under Marie Skłodowska-Curie Grant Agreement No. 699935. We acknowledge additional support from the Alvin L. and Verla R. Kwiram Endowment from the Department of Chemistry at the University of Washington. Theoretical study of defects is supported by the University of Washington Molecular Engineering Materials Center funded by the NSF (DMR-1719797 and CHE-1565520).

■ REFERENCES

(1) Rong, Y.; Liu, L.; Mei, A.; Li, X.; Han, H. Beyond Efficiency: the Challenge of Stability in Mesoscopic Perovskite Solar Cells. *Adv. Energy Mater.* **2015**, *5*, 1501066.

(2) Berhe, T. A.; Su, W.-N.; Chen, C.-H.; Pan, C.-J.; Cheng, J.-H.; Chen, H.-M.; Tsai, M.-C.; Chen, L.-Y.; Dubale, A. A.; Hwang, B.-J. Organometal Halide Perovskite Solar Cells: Degradation and Stability. *Energy Environ. Sci.* **2016**, *9*, 323−356.

(3) Yuan, Y.; Huang, J. Ion Migration in Organometal Trihalide Perovskite and Its Impact on Photovoltaic Efficiency and Stability. *Acc. Chem. Res.* **2016**, *49*, 286−293.

(4) Xiao, Z.; Yuan, Y.; Shao, Y.; Wang, Q.; Dong, Q.; Bi, C.; Sharma, P.; Gruverman, A.; Huang, J. Giant Switchable Photovoltaic Effect in Organometal Trihalide Perovskite Devices. *Nat. Mater.* **2015**, *14*, 193−198.

(5) Yuan, Y.; Chae, J.; Shao, Y.; Wang, Qi; Xiao, Z.; Centrone, A.; Huang, J. Photovoltaic Switching Mechanism in Lateral Structure Hybrid Perovskite Solar Cells. *Adv. Energy Mater.* **2015**, *5*, 1500615.

(6) deQuilettes, D. W.; Zhang, W.; Burlakov, V. M.; Graham, D. J.; Leijtens, T.; Osherov, A.; Bulovic, V.; Snaith, H. J.; Ginger, D. S.; Stranks, S. D. Photo-Induced Halide Redistribution in Organic-Inorganic Perovskite Films. *Nat. Commun.* **2016**, *7*, 11683.

(7) Yang, T. Y.; Gregori, G.; Pellet, N.; Gratzel, M.; Maier, J. The Significance of Ion Conduction in a Hybrid Organic-Inorganic Lead-Iodide-Based Perovskite Photosensitizer. *Angew. Chem., Int. Ed.* **2015**, *54*, 7905−7910.

DOI: 10.1021/acsenergylett.8b00505
ACS Energy Lett. 2018, 3, 1279−1286

(8) Walsh, A.; Scanlon, D. O.; Chen, S.; Gong, X. G.; Wei, S.-H. Self-Regulation Mechanism for Charged Point Defects in Hybrid Halide Perovskites. *Angew. Chem., Int. Ed.* **2015**, *54*, 1791−1794.
(9) Domanski, K.; Roose, B.; Matsui, T.; Saliba, M.; Turren-Cruz, S.-H.; Correa-Baena, J.-P.; Carmona, C. R.; Richardson, G.; Foster, J. M.; De Angelis, F.; et al. Migration of Cations Induces Reversible Performance Losses Over Day/Night Cycling in Perovskite Solar Cells. *Energy Environ. Sci.* **2017**, *10*, 604−613.
(10) Unger, E. L.; Hoke, E. T.; Bailie, C. D.; Nguyen, W. H.; Bowring, A. R.; Heumüller, T.; Christoforo, M. G.; McGehee, M. D. Hysteresis and Transient Behavior in Current−Voltage Measurements of Hybrid-Perovskite Absorber Solar Cells. *Energy Environ. Sci.* **2014**, *7*, 3690−3698.
(11) Tress, W.; Marinova, N.; Moehl, T.; Zakeeruddin, S. M.; Nazeeruddin, M. K.; Grätzel, M. Understanding the Rate-Dependent J−V Hysteresis, Slow Time Component, and Aging in $CH_3NH_3PbI_3$ Perovskite Solar Cells: The Role of a Compensated Electric Field. *Energy Environ. Sci.* **2015**, *8*, 995−1004.
(12) Pockett, A.; Eperon, G. E.; Sakai, N.; Snaith, H. J.; Peter, L. M.; Cameron, P. J. Microseconds, Milliseconds and Seconds: Deconvoluting the Dynamic Behaviour of Planar Perovskite Solar Cells. *Phys. Chem. Chem. Phys.* **2017**, *19*, 5959−5970.
(13) Yoon, S. J.; Draguta, S.; Manser, J. S.; Sharia, O.; Schneider, W. F.; Kuno, M.; Kamat, P. V. Tracking Iodide and Bromide Ion Segregation in Mixed Halide Lead Perovskites during Photoirradiation. *ACS Energy Lett.* **2016**, *1*, 290−296.
(14) Gratia, P.; Grancini, G.; Audinot, J. N.; Jeanbourquin, X.; Mosconi, E.; Zimmermann, I.; Dowsett, D.; Lee, Y.; Gratzel, M.; De Angelis, F.; et al. Intrinsic Halide Segregation at Nanometer Scale Determines the High Efficiency of Mixed Cation/Mixed Halide Perovskite Solar Cells. *J. Am. Chem. Soc.* **2016**, *138*, 15821−15824.
(15) Stranks, S. D.; Burlakov, V. M.; Leijtens, T.; Ball, J. M.; Goriely, A.; Snaith, H. J. Recombination Kinetics in Organic-Inorganic Perovskites: Excitons, Free Charge, and Subgap States. *Phys. Rev. Appl.* **2014**, *2*, 034007−034007.
(16) Tian, Y.; Peter, M.; Unger, E.; Abdellah, M.; Zheng, K.; Pullerits, T.; Yartsev, A.; Sundstrom, V.; Scheblykin, I. G. Mechanistic Insights into Perovskite Photoluminescence Enhancement: Light Curing with Oxygen can Boost Yield Thousandfold. *Phys. Chem. Chem. Phys.* **2015**, *17*, 24978−24987.
(17) Deng, X.; Wen, X.; Lau, C. F. J.; Young, T.; Yun, J.; Green, M. A.; Huang, S.; Ho-Baillie, A. W. Y. Electric Field Induced Reversible and Irreversible Photoluminescence Responses in Methylammonium Lead Iodide Perovskite. *J. Mater. Chem. C* **2016**, *4*, 9060−9068.
(18) Zhao, Y.; Zhou, W.; Ma, W.; Meng, S.; Li, H.; Wei, J.; Fu, R.; Liu, K.; Yu, D.; Zhao, Q. Correlations between Immobilizing Ions and Suppressing Hysteresis in Perovskite Solar Cells. *ACS Energy Lett.* **2016**, *1*, 266−272.
(19) Li, C.; Guerrero, A.; Zhong, Y.; Graser, A.; Luna, C. A. M.; Kohler, J.; Bisquert, J.; Hildner, R.; Huettner, S. Real-Time Observation of Iodide Ion Migration in Methylammonium Lead Halide Perovskites. *Small* **2017**, *13*, 1701711.
(20) Buin, A.; Pietsch, P.; Xu, J.; Voznyy, O.; Ip, A. H.; Comin, R.; Sargent, E. H. Materials Processing Routes to Trap-Free Halide Perovskites. *Nano Lett.* **2014**, *14*, 6281−6286.
(21) Kim, J.; Lee, S. H.; Lee, J. H.; Hong, K. H. The Role of Intrinsic Defects in Methylammonium Lead Iodide Perovskite. *J. Phys. Chem. Lett.* **2014**, *5*, 1312−1317.
(22) Yin, W.-J.; Shi, T.; Yan, Y. Unusual Defect Physics in $CH_3NH_3PbI_3$ Perovskite Solar Cell Absorber. *Appl. Phys. Lett.* **2014**, *104*, 063903.
(23) Tress, W. Metal Halide Perovskites as Mixed Electronic-Ionic Conductors: Challenges and Opportunities-From Hysteresis to Memristivity. *J. Phys. Chem. Lett.* **2017**, *8*, 3106−3114.
(24) Jacobs, D. L.; Scarpulla, M. A.; Wang, C.; Bunes, B. R.; Zang, L. Voltage-Induced Transients in Methylammonium Lead Triiodide Probed by Dynamic Photoluminescence Spectroscopy. *J. Phys. Chem. C* **2016**, *120*, 7893−7902.
(25) Calado, P.; Telford, A. M.; Bryant, D.; Li, X.; Nelson, J.; O'Regan, B. C.; Barnes, P. R. F. Evidence for Ion Migration in Hybrid Perovskite Solar Cells with Minimal Hysteresis. *Nat. Commun.* **2016**, *7*, 13831.
(26) van Reenen, S.; Kemerink, M.; Snaith, H. J. Modeling Anomalous Hysteresis in Perovskite Solar Cells. *J. Phys. Chem. Lett.* **2015**, *6*, 3808−3814.
(27) Wehrenfennig, C.; Eperon, G. E.; Johnston, M. B.; Snaith, H. J.; Herz, L. M. High Charge Carrier Mobilities and Lifetimes in Organolead Trihalide Perovskites. *Adv. Mater.* **2014**, *26*, 1584−1589.
(28) Stranks, S. D.; Eperon, G. E.; Grancini, G.; Menelaou, C.; Alcocer, M. J. P.; Leijtens, T.; Herz, L. M.; Petrozza, A.; Snaith, H. J. Electron-Hole Diffusion Lengths Exceeding 1Micrometer in an Organometal Trihalide Perovskite Absorber. *Science* **2013**, *342*, 341−344.
(29) Milot, R. L.; Eperon, G. E.; Snaith, H. J.; Johnston, M. B.; Herz, L. M. Temperature-Dependent Charge-Carrier Dynamics in $CH_3NH_3PbI_3$ Perovskite Thin Films. *Adv. Funct. Mater.* **2015**, *25*, 6218−6227.
(30) Edri, E.; Kirmayer, S.; Henning, A.; Mukhopadhyay, S.; Gartsman, K.; Rosenwaks, Y.; Hodes, G.; Cahen, D. Why lead methylammonium tri-iodide perovskite-based solar cells require a mesoporous electron transporting scaffold (but not necessarily a hole conductor). *Nano Lett.* **2014**, *14*, 1000−1004.
(31) deQuilettes, D. W.; Koch, S.; Burke, S.; Paranji, R. K.; Shropshire, A. J.; Ziffer, M. E.; Ginger, D. S. Photoluminescence Lifetimes Exceeding 8 μs and Quantum Yields Exceeding 30% in Hybrid Perovskite Thin Films by Ligand Passivation. *ACS Energy Lett.* **2016**, *1*, 438−444.
(32) Noel, N. K.; Abate, A.; Stranks, S. D.; Parrott, E. S.; Burlakov, V. M.; Goriely, A.; Snaith, H. J. Enhanced Photoluminescence and Solar Cell Performance via Lewis Base Passivaation of Organic-Inorganic Lead Halide Perovskites. *ACS Nano* **2014**, *8*, 9815−9821.
(33) Zhang, Y.; Wang, Y.; Xu, Z. Q.; Liu, J.; Song, J.; Xue, Y.; Wang, Z.; Zheng, J.; Jiang, L.; Zheng, C.; et al. Reversible Structural Swell-Shrink and Recoverable Optical Properties in Hybrid Inorganic-Organic Perovskite. *ACS Nano* **2016**, *10*, 7031−7038.
(34) Mosconi, E.; Meggiolaro, D.; Snaith, H. J.; Stranks, S. D.; De Angelis, F. Light-Induced Annihilation of Frenkel Defects in Organo-Lead Halide Perovskites. *Energy Environ. Sci.* **2016**, *9*, 3180−3187.
(35) deQuilettes, D. W.; Vorpahl, S. M.; Stranks, S. D.; Nagaoka, H.; Eperon, G. E.; Ziffer, M. E.; Snaith, H. J.; Ginger, D. S. Impact of Microstructure on Local Carrier Lifetime in Perovskite Solar Cells. *Science* **2015**, *348*, 683−686.
(36) deQuilettes, D. W.; Jariwala, S.; Burke, S.; Ziffer, M. E.; Wang, J. T.; Snaith, H. J.; Ginger, D. S. Tracking Photoexcited Carriers in Hybrid Perovskite Semiconductors: Trap-Dominated Spatial Heterogeneity and Diffusion. *ACS Nano* **2017**, *11*, 11488−11496.
(37) Bischak, C. G.; Sanehira, E. M.; Precht, J. T.; Luther, J. M.; Ginsberg, N. S. Heterogeneous Charge Carrier Dynamics in Organic-Inorganic Hybrid Materials: Nanoscale Lateral and Depth-Dependent Variation of Recombination Rates in Methylammonium Lead Halide Perovskite Thin Films. *Nano Lett.* **2015**, *15*, 4799−4807.
(38) Leijtens, T.; Srimath Kandada, A. R.; Eperon, G. E.; Grancini, G.; D'Innocenzo, V.; Ball, J. M.; Stranks, S. D.; Snaith, H. J.; Petrozza, A. Modulating the Electron-Hole Interaction in a Hybrid Lead Halide Perovskite with an Electric Field. *J. Am. Chem. Soc.* **2015**, *137*, 15451−15459.
(39) Pingree, L. S. C.; Rodovsky, D. B.; Coffey, D. C.; Bartholomew, G. P.; Ginger, D. S. Scanning Kelvin Probe Imaging of the Potential Profiles in Fixed and Dynamic Planar LECs. *J. Am. Chem. Soc.* **2007**, *129*, 15903−15910.
(40) Rodovsky, D. B.; Reid, O. G.; Pingree, L. S. C.; Ginger, D. S. Concerted Emission and Local Potentiometry of Light-Emitting Electrochemical Cells. *ACS Nano* **2010**, *4*, 2673−2680.
(41) Slinker, J. D.; DeFranco, J. A.; Jaquith, M. J.; Silveira, W. R.; Zhong, Y. W.; Moran-Mirabal, J. M.; Craighead, H. G.; Abruna, H. D.; Marohn, J. A.; Malliaras, G. G. Direct Measurement of the Electric-

DOI: 10.1021/acsenergylett.8b00505
ACS Energy Lett. 2018, 3, 1279−1286

Field Distribution in a Light-Emitting Electrochemical Cell. *Nat. Mater.* **2007**, *6*, 894−899.
(42) Bergmann, V. W.; Weber, S. A.; Javier Ramos, F.; Nazeeruddin, M. K.; Gratzel, M.; Li, D.; Domanski, A. L.; Lieberwirth, I.; Ahmad, S.; Berger, R. Real-Space Observation of Unbalanced Charge Distribution Inside a Perovskite-Sensitized Solar Cell. *Nat. Commun.* **2014**, *5*, 5001.
(43) Collins, S. D.; Mikhnenko, O. V.; Nguyen, T. L.; Rengert, Z. D.; Bazan, G. C.; Woo, H. Y.; Nguyen, T.-Q. Observing Ion Motion in Conjugated Polyelectrolytes with Kelvin Probe Force Microscopy. *Adv. Elect. Mater.* **2017**, *3*, 1700005.
(44) Pingree, L. S. C.; Reid, O. G.; Ginger, D. S. Electrical Scanning Probe Microscopy on Active Organic Electronic Devices. *Adv. Mater.* **2009**, *21*, 19−28.
(45) Stoumpos, C. C.; Malliakas, C. D.; Kanatzidis, M. G. Semiconducting Tin and Lead Iodide Perovskites with Organic Cations: Phase Transitions, High Mobilities, and Near-Infrared Photoluminescent Properties. *Inorg. Chem.* **2013**, *52*, 9019−9038.
(46) Bergmann, V. W.; Guo, Y.; Tanaka, H.; Hermes, I. M.; Li, D.; Klasen, A.; Bretschneider, S. A.; Nakamura, E.; Berger, R.; Weber, S. A. Local Time-Dependent Charging in a Perovskite Solar Cell. *ACS Appl. Mater. Interfaces* **2016**, *8*, 19402−19409.
(47) Brivio, F.; Butler, K. T.; Walsh, A.; van Schilfgaarde, M. Relativistic Quasiparticle Self-Consistent Electronic Structure of Hybrid Halide Perovskite Photovoltaic Absorbers. *Phys. Rev. B: Condens. Matter Mater. Phys.* **2014**, *89*, 155204.
(48) Draguta, S.; Thakur, S.; Morozov, Y. V.; Wang, Y.; Manser, J. S.; Kamat, P. V.; Kuno, M. Spatially Non-uniform Trap State Densities in Solution-Processed Hybrid Perovskite Thin Films. *J. Phys. Chem. Lett.* **2016**, *7*, 715−721.
(49) Sugimura, H.; Ishida, Y.; Hayashi, K.; Takai, O.; Nakagiri, N. Potential Shielding by the Surface Water Layer in Kelvin Probe Force Microscopy. *Appl. Phys. Lett.* **2002**, *80*, 1459−1461.
(50) Agiorgousis, M. L.; Sun, Y. Y.; Zeng, H.; Zhang, S. Strong Covalency-Induced Recombination Centers in Perovskite Solar Cell Material $CH_3NH_3PbI_3$. *J. Am. Chem. Soc.* **2014**, *136*, 14570−14575.
(51) Yin, W. J.; Shi, T.; Yan, Y. Unique Properties of Halide Perovskites as Possible Origins of the Superior Solar Cell Performance. *Adv. Mater.* **2014**, *26*, 4653−4658.
(52) Lindblad, R.; Bi, D.; Park, B. W.; Oscarsson, J.; Gorgoi, M.; Siegbahn, H.; Odelius, M.; Johansson, E. M.; Rensmo, H. Electronic Structure of $TiO_2/CH_3NH_3PbI_3$ Perovskite Solar Cell Interfaces. *J. Phys. Chem. Lett.* **2014**, *5*, 648−653.
(53) Conings, B.; Baeten, L.; De Dobbelaere, C.; D'Haen, J.; Manca, J.; Boyen, H. G. Perovskite-Based Hybrid Solar Cells Exceeding 10% Efficiency with High Reproducibility Using a Thin Film Sandwich Approach. *Adv. Mater.* **2014**, *26*, 2041−2046.
(54) Raga, S. R.; Jung, M.-C.; Lee, M. V.; Leyden, M. R.; Kato, Y.; Qi, Y. Influence of Air Annealing on High Efficiency Planar Structure Perovskite Solar Cells. *Chem. Mater.* **2015**, *27*, 1597−1603.
(55) Sadoughi, G.; Starr, D. E.; Handick, E.; Stranks, S. D.; Gorgoi, M.; Wilks, R. G.; Bar, M.; Snaith, H. J. Observation and Mediation of the Presence of Metallic Lead in Organic-Inorganic Perovskite Films. *ACS Appl. Mater. Interfaces* **2015**, *7*, 13440−13444.
(56) Qin, C.; Matsushima, T.; Fujihara, T.; Adachi, C. Multifunctional Benzoquinone Additive for Efficient and Stable Planar Perovskite Solar Cells. *Adv. Mater.* **2017**, *29*, 1603808.
(57) Senocrate, A.; Moudrakovski, I.; Kim, G. Y.; Yang, T. Y.; Gregori, G.; Gratzel, M.; Maier, J. The Nature of Ion Conduction in Methylammonium Lead Iodide: A Multimethod Approach. *Angew. Chem., Int. Ed.* **2017**, *56*, 7755−7759.
(58) Liu, N.; Yam, C. First-Principles Study of Intrinsic Defects in Formamidinium Lead Triiodide Perovskite Solar Cell Absorbers. *Phys. Chem. Chem. Phys.* **2018**, *20*, 6800−6804.

DOI: 10.1021/acsenergylett.8b00505
ACS Energy Lett. 2018, 3, 1279−1286